A sample of radio-loud active galactic nuclei in the Sloan Digital Sky Survey

P. N. Best,[1][*] G. Kauffmann,[2] T. M. Heckman[3] and Ž. Ivezić[4]

[1]*Institute for Astronomy, Royal Observatory Edinburgh, Blackford Hill, Edinburgh EH9 3HJ*
[2]*Max-Planck-Institut für Astrophysik, Karl-Schwarzschild-Strasse 1, D-85748 Garching, Germany*
[3]*Department of Physics & Astronomy, The Johns Hopkins University, Baltimore, MD 21218, USA*
[4]*Princeton University Observatory, Peyton Hall, Princeton, NJ 08544-1001, USA*

ABSTRACT

A sample of 2712 radio-luminous galaxies is defined from the second data release of the Sloan Digital Sky Survey (SDSS) by cross-comparing the main spectroscopic galaxy sample with two radio surveys: the National Radio Astronomy Observatories (NRAO) Very Large Array (VLA) Sky Survey (NVSS) and the Faint Images of the Radio Sky at Twenty centimeters (FIRST) survey. The comparison is carried out in a multistage process and makes optimal use of both radio surveys by exploiting the sensitivity of the NVSS to extended and multicomponent radio sources in addition to the high angular resolution of the FIRST images. A radio source sample with 95 per cent completeness and 98.9 per cent reliability is achieved, far better than would be possible for this sample if only one of the surveys was used. The radio source sample is then divided into two classes: radio-loud active galactic nuclei (AGN) and galaxies in which the radio emission is dominated by star formation. The division is based on the location of a galaxy in the plane of 4000-Å break strength versus radio luminosity per unit stellar mass and provides a sample of 2215 radio-loud AGN and 497 star-forming galaxies brighter than 5 mJy at 1.4 GHz. A full catalogue of positions and radio properties is provided for these sources. The local radio luminosity function is then derived both for radio-loud AGN and for star-forming galaxies and is found to be in agreement with previous studies. By using the radio to far-infrared (FIR) correlation, the radio luminosity function of star-forming galaxies is also compared to the luminosity function derived in the FIR. It is found to agree well at high luminosities but less so at lower luminosities, confirming that the linearity of the radio to FIR correlation breaks down below about 10^{22} W Hz^{-1} at 1.4 GHz.

Key words: surveys – galaxies: active – galaxies: evolution – galaxies: luminosity function, mass function – galaxies: starburst – radio continuum: galaxies.

1 INTRODUCTION

In recent years, new radio surveys such as the National Radio Astronomy Observatory (NRAO) Very Large Array (VLA) Sky Survey (NVSS; Condon et al. 1998, and the Faint Images of the Radio Sky at Twenty centimeters (FIRST) survey (Becker, White & Helfand 1995) have covered substantial fractions of the sky down to milli-Jansky flux densities, at vastly higher angular resolution than their predecessors. Such radio surveys are dramatically advancing our understanding of extragalactic radio sources, by permitting detailed statistical studies to be carried out. In order to reap the full benefit of these surveys, it is necessary to optically identify the radio sources, so as to obtain spectroscopic redshifts and determine the properties of their host galaxies. The availability of new large galaxy redshift surveys, especially the 2-degree Field Galaxy Redshift Survey (2dFGRS; Colless et al. 2001) and the Sloan Digital Sky Survey (SDSS; York et al. 2000; Stoughton et al. 2002), means that optical identifications and redshifts are available for large samples of nearby radio sources and allows comprehensive statistical analyses of their host galaxy properties to be carried out.

Automated cross-correlation of surveys across different wavelength regimes has a long history in astronomy. It is important that this process should maximize both the completeness and the reliability of the resulting sample, so considerable care needs to be taken in choosing the parameters that determine whether objects in different catalogues are indeed associated. In the case of optical identification of radio sources, the choice of radio survey is important. This is because many radio sources are extended, with sizes from a few arcsec up to tens of arcmin, and in high angular

resolution surveys different components of the same source may be resolved into distinct sources. Surveys at lower angular resolution detect most sources as single components, and also have good sensitivity to extended radio structures, but the high surface density of possible optical counterparts (over 4000 per square degree at high Galactic latitudes in the Palomar Observatory Sky Survey) limits the reliability of the optical matching.

The first radio sky surveys were carried out at very low angular resolution and detected only the brightest radio sources. The resolution of these surveys was too low to allow identification of the host galaxies without detailed radio follow-up observations of the detected sources; this was time-consuming and meant that only small samples of galaxies could be studied (see discussion in McMahon et al. 2002). The NVSS was the first radio survey of sufficiently high angular resolution (45 arcsec) to permit automated cross-correlation with optical surveys. Machalski & Condon (1999) cross-correlated the NVSS with the Las Campanas Redshift Survey (LCRS; Shectman et al. (1997)), identifying 1157 radio-emitting galaxies. Machalski & Godlowski (2000) used this sample to derive the local radio luminosity function. Using far-infrared (FIR) data available for the LCRS they were also able to separate the luminosity function into a radio-loud active galactic nuclei (AGN) component, which dominates at high radio luminosities, and a lower luminosity component due to star-forming galaxies that emit in the radio predominantly due to the synchrotron emission from supernova remnants. Similarly, Sadler et al. (2002) cross-correlated the NVSS with galaxies from the first data release of the 2dFGRS, defining a sample of 912 radio sources which form a basis for further detailed studies (e.g. Best 2004).

The 45-arcsec resolution of the NVSS has the advantage of being sufficiently large that ∼99 per cent of radio sources are contained within a single NVSS component. With the exception of a few very large sources, the NVSS is also able to detect the entirety of the radio emission. However, the poor angular resolution of the NVSS leads to significant uncertainties in cross-identifying the radio sources with their optical host galaxies and there is a trade-off between the reliability of the matched sample and its completeness. Sadler et al. (2002) accepted radio sources within a matching radius of 10 arcsec from an optical galaxy, leading to a catalogue that was ∼90 per cent complete, but in which 5–10 per cent of the matches are expected to be false identifications.

Samples with much higher reliability can be derived using the FIRST catalogue, due to its superior angular resolution (∼5 arcsec). Ivezić et al. (2002) cross-correlated the FIRST survey with the SDSS imaging sample. Under the assumption that all true identifications of point radio sources would have radio-optical positional offsets of less than 3 arcsec, they concluded that the optimal matching radius for cross-correlation was 1.5 arcsec, for which they derived a completeness for radio point sources of 85 per cent and a contamination rate of only 3 per cent.

However, at the high angular resolution of FIRST, new problems arise. FIRST is not sensitive to extended radio structures because of a lack of short antennae baselines, and resolves out the extended emission of radio sources. As a result, the total radio luminosity of sources that are larger than a few arcseconds will be systematically low (cf. Becker et al. 1995). In extreme cases, some larger radio sources are missed. These effects introduce systematic biases into the derived radio source sample. In addition, many extended radio sources are split into multiple components by FIRST. Matching routines therefore need to be developed to account for the possible multicomponent nature of radio sources.

The first attempt to automate such a routine was by Magliocchetti et al. (1998), who used a 'collapsing algorithm' to identify multi-component FIRST sources. They considered all pairs of sources with separations below 3 arcmin, and merged into a single combined source all pairs with separations below 100 $(S_{tot}/100\,mJy)^{0.5}$ arcsec and flux densities within a factor of 4 of each other. This method is simple and works well for classical double-lobed radio sources, but accounts poorly for core-jet sources or sources with large asymmetries.

Ivezić et al. (2002) improved on this by first cross-correlating all FIRST sources with the SDSS (thereby picking up all sources with a core component) and then adding candidate double-lobed radio sources to this sample. These were identified by comparing the mid-points of all FIRST pairs with separations below 90 arcsec with the galaxies in the optical catalogue, and accepting all matches with offsets below 3 arcsec. They estimated that such double sources contribute less than 10 per cent of all radio sources.

McMahon et al. (2002) carried out a detailed study of the properties of multicomponent FIRST sources by comparing isolated pairs of FIRST sources with optical Automated Plate Measuring Machine (APM) scans of the Palomar Observatory Sky Survey (POSS) plates. For core-jet type sources, where the optical counterpart is associated with one of the radio components, they found that the radio components usually have very different flux densities and that the component with the optical counterpart is usually brighter and is frequently unresolved in the radio. In contrast, if the optical counterpart is located between the two radio components, the two radio components usually have comparable flux densities and similar radio sizes (i.e. both are consistent with being radio lobes, not one unresolved core and an extended radio lobe). In this case, the optically identified galaxy is typically located fairly close to the flux-weighted mean position of the two radio components. This information is extremely useful in the identification of multicomponent FIRST sources.

As the main spectroscopic galaxy sample of the SDSS has rather low median redshift ($z \sim 0.1$), the problems described above associated with identifying extended radio sources will be more severe. This paper thus presents a hybrid method, using information from both NVSS and FIRST in order to take advantage of the strong points of both surveys and avoid the systematic errors that arise in using only one of them. The layout of the paper is as follows. In Section 2, the salient points of the SDSS, NVSS and FIRST surveys are summarized. Section 3 then discusses the cross-matching of these surveys to identify the radio source sample. Section 4 describes how true radio-loud AGN are separated from sources where the radio emission is associated with star formation activity. The local radio luminosity functions of radio-loud AGN and star-forming galaxies are derived in Section 5, and the radio luminosity function of star-forming galaxies is compared to that derived at FIR wavelengths. Conclusions are drawn in Section 6. In an accompanying paper (Best et al. 2005) the host galaxies of the radio-loud AGN are investigated in detail. Throughout the paper, the values adopted for the cosmological parameters are $\Omega_m = 0.3$, $\Omega_\Lambda = 0.7$, and $H_0 = 70\,km\,s^{-1}\,Mpc^{-1}$.

2 THE RADIO AND OPTICAL GALAXY SAMPLES

2.1 The SDSS spectroscopic sample

The Sloan Digital Sky Survey (York et al. 2000; Stoughton et al. 2002, and references therein) is an optical imaging (u,g,r,i,z bands) and spectroscopic survey of about a quarter of the extragalactic sky,

being carried out at the Apache Point Observatory. The spectroscopic sample considered in this paper is a sample of about 212 000 objects with magnitudes $14.5 < r < 17.77$, spectroscopically confirmed to be galaxies, drawn from the 'main galaxy catalogue' of the second data release (DR2) of the SDSS. This sample of galaxies is described by Brinchmann et al. (2004a). The galaxies have a median redshift of $z \sim 0.1$.

The SDSS spectra cover an observed wavelength range of 3800–9200 Å, at an instrumental velocity resolution of about $65 \, \mathrm{km \, s^{-1}}$. The spectra are obtained through 3-arcsec diameter fibres, which corresponds to 5.7 kpc at a redshift of 0.1; at this redshift the spectra therefore represent a large proportion (up to 50 per cent) of the total galaxy light, while for the very lowest redshift objects they are more dominated by the nuclear emission.

As described in Brinchmann et al. (2004a), a variety of physical parameters for these galaxies have been derived from the photometric and spectroscopic data, and catalogues of these parameters are publicly available. These include total stellar masses, mass-to-light ratios, 4000-Å break strengths, Hδ absorption measurements and estimates of dust attenuation (Kauffmann et al. 2003a,b); accurate emission-line fluxes, after subtraction of the modelled stellar continuum to account for underlying stellar absorption features (Kauffmann et al. 2003c; Tremonti et al. in preparation); galaxy metallicities (Tremonti et al. 2004); parameters measuring optical AGN activity, such as emission-line ratios, and galaxy velocity dispersions (hence black hole mass estimates; Kauffmann et al. 2003c; Heckman et al. 2004). These parameters have been adopted for the analyses of this paper: the reader is referred to the papers referenced above for detailed information about the methods used to derive them.

It should be emphasized that the use of the SDSS main galaxy catalogue as the basis sample for this study means that objects classified as 'quasars' by the automated SDSS classification pipeline (Schlegel et al. in preparation) are excluded. These objects are excluded because of the influence of the direct non-stellar continuum light from the active nucleus. This affects the observed optical magnitudes, preventing clean magnitude-limited samples from being derived, and prohibits the host galaxy parameters discussed above from being accurately determined. The number of AGN excluded in this way is very small ($\lesssim 3$ per cent out to $z = 0.1$),[1] because this exclusion only applies to the most luminous Type I AGN: the SDSS pipeline classifies most low luminosity Type I AGN as 'galaxies' rather than 'quasars', and so they are retained. Kauffmann et al. (2003c) estimate that 8 per cent of AGN in the main galaxy sample have broad emission lines, and therefore are strictly Type Is. They also demonstrate that for these low luminosity objects the non-stellar continuum light has a negligible effect on the physical parameters derived for the host galaxy.

2.2 The NVSS and FIRST radio surveys

The NVSS (Condon et al. 1998) and FIRST (Becker et al. 1995) surveys are two radio surveys that have been carried out in recent years using the VLA radio synthesis telescope at a frequency of 1.4 GHz. The NVSS was observed with the array in D configuration (DnC configuration for the most southerly fields), which provides an angular resolution of 45 arcsec. This survey covers the entirety of

the sky north of $-40°$ declination, down to a limiting point source flux density of about 2.5 mJy. The FIRST observations were carried out in B-array configuration, which provides a much higher angular resolution of $\sim$5 arcsec. This survey was designed to study the region of sky that will be observed by the SDSS, and therefore overlaps with this very closely. It reaches a limiting flux density of about 1 mJy for point sources.

3 CROSS-MATCHING OF THE SDSS SPECTROSCOPIC SAMPLE USING A COMBINATION OF NVSS AND FIRST

The FIRST and NVSS surveys are highly complementary for identifying radio sources associated with nearby galaxies; NVSS provides the sensitivity to large-scale radio structures required to detect all of the emission from extended radio sources, while FIRST provides the high angular resolution required to reliably identify the host galaxy. In order to identify radio sources associated with galaxies in the SDSS spectroscopic sample, a hybrid method using both radio surveys has been derived. A broad overview of the steps in this process is as follows.

(1) SDSS galaxies lying outside the sky coverage of the FIRST survey were excluded. Galaxies close to very bright radio sources were also excluded, because the noise of the NVSS images is much greater in these regions. Finally, galaxies with redshifts below 0.01 were excluded, because at these low redshifts the galaxies are very extended and their optical positions are consequently uncertain.

(2) The remaining sample was cross-correlated with the NVSS catalogue. A list of candidate galaxies that might be associated with multi-NVSS-component radio sources was derived.

(3) These multi-NVSS-component candidates were investigated; by necessity, a small proportion of this analysis had to be done visually rather than through automated procedures. If a galaxy was confirmed to be associated with a multi-NVSS-component source, the integrated flux densities of the NVSS components were summed to provide the radio source flux density.

(4) All galaxies matched with a single NVSS source were then cross-correlated with the FIRST catalogue. Note, however, that the presence of a FIRST counterpart was not *required* for a source to be accepted. If there was no FIRST counterpart, then the source was accepted or rejected solely upon its NVSS properties.

(5) If a single FIRST counterpart was associated with the NVSS source, then the source was accepted or rejected on the basis of the properties of the FIRST counterpart. For accepted matches, however, the adopted radio flux density was taken from the NVSS data.

(6) If multiple FIRST components were associated with the NVSS source, then the source was accepted if it satisfied criteria for a single-component source (with unrelated additional FIRST sources) or for a radio source with multiple FIRST components. Again, the NVSS catalogue was used to provide the most accurate measure of the radio flux density.

The exact criteria for accepting and rejecting matches in the procedures outlined above were tested and refined using Monte-Carlo simulations. Ten catalogues of random sky locations were constructed, over the same sky area as the SDSS survey. Each catalogue contained the same number as positions as the list of SDSS galaxies, and these random catalogues were taken through exactly the same steps of cross-comparison with the radio data as the SDSS galaxy catalogue. In the subsections that follow, the resulting optimal selection criteria are described, together with the completeness and reliability estimates provided by the Monte Carlo simulations.

---

[1] A search of the SDSS DR2 data base reveals only 393 objects classified as 'quasars' in the redshift range $0.03 < z < 0.1$, compared to 16 661 objects classified as emission-line AGN by Kauffmann et al. (2003c).

Note that the flux densities adopted for the NVSS sources are true integrated flux densities, rather than the peak flux densities quoted in the NVSS catalogues. The formulae for conversion of peak flux densities to integrated flux densities are provided by Condon et al. (1998). Only those radio sources with total flux densities (after summing NVSS components if necessary) above 5 mJy are retained. This flux density limit corresponds to approximately 10 times the noise level of the NVSS maps, and is adopted because: (i) at this significance level, all sources should be real and have well determined positions; (ii) at this flux density limit, the sample is as sensitive to extended single-component NVSS sources (which will have a lower peak flux density) as it is to point sources, and the sensitivity to multicomponent NVSS sources will not be significantly worse (for example, a 5 mJy source composed of two individual components of 2.5 mJy would be found). The 5 mJy limit corresponds to about 10^{23} W Hz^{-1} at redshift $z \sim 0.1$, which is approximately where the radio luminosity function switches from being dominated by star-forming galaxies (low luminosities) to being dominated by AGN (high luminosities).

3.1 Identification of multicomponent NVSS sources

In order to search for possible multicomponent NVSS sources, a search was made for multiple sources within a radius of 3 arcmin from each optical galaxy. This distance was selected to be large enough that any genuine multicomponent radio source should have at least two matches, but still much smaller than the typical separation of NVSS sources (8–10 arcmin).

3.1.1 Candidate NVSS doubles

For galaxies with two NVSS matches within 3 arcmin, the top panels of Fig. 1 compare the offsets of the two NVSS matches from the optical position for SDSS galaxies (left) and for an equivalent number of random positions (right). There are a large number of SDSS galaxies for which the nearer NVSS component lies within 15 arcsec of the optical galaxy; these are predominantly galaxies containing a single-component NVSS source and the other NVSS source is physically unrelated. Such sources were classified as single-component matches (see below).
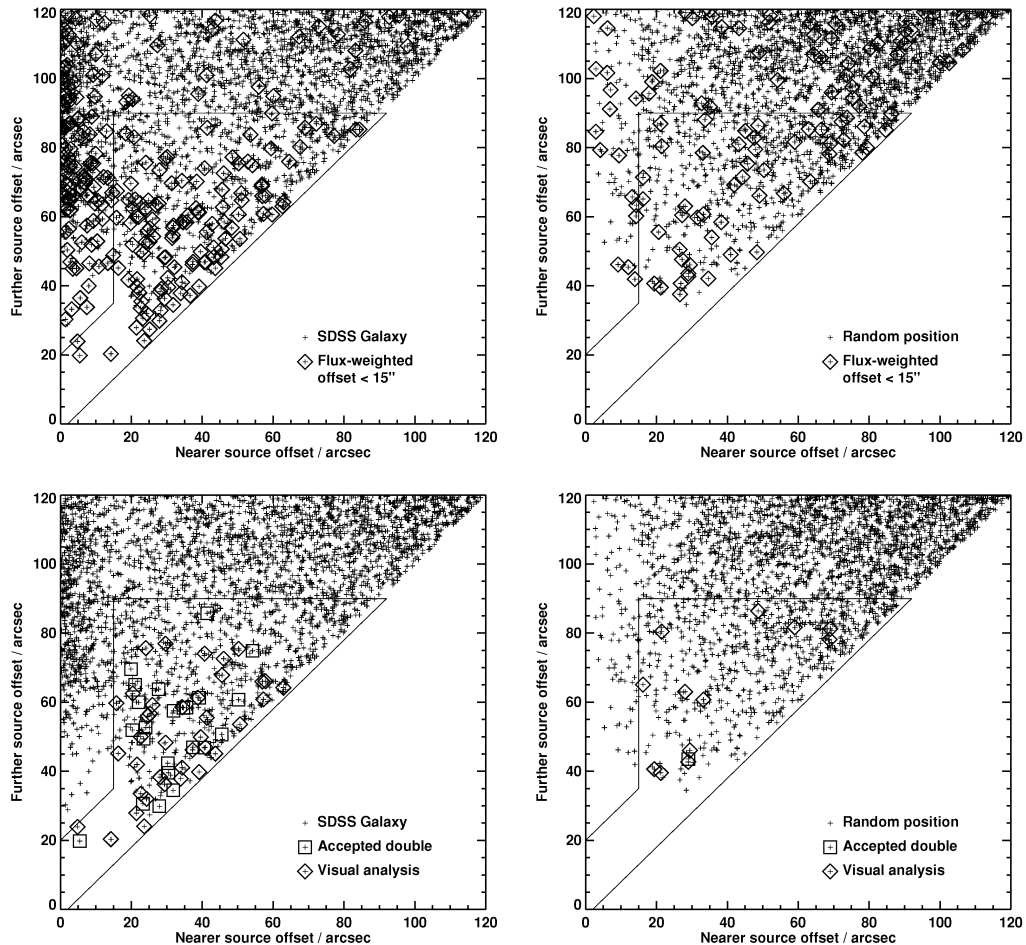

Figure 1. For those SDSS galaxies (left) and an equivalent number of random positions (right) which have two NVSS sources within 3 arcmin, the plots show the positional offsets of the two NVSS sources from the optical galaxy or random position. In the upper panels, the diamonds indicate those cases where the flux-weighted mean position of the two NVSS sources is within 15 arcsec of the optical/random position. The solid lines enclose the region in which large numbers of candidate double sources are found, without being swamped by false identifications. The lower plots then show the result of comparing these candidate doubles with the FIRST catalogue. The criteria for the candidates to be accepted, rejected or referred to visual analysis are described in the text: this leads to a number of accepted doubles (with very few false detections), and a small sample of sources to be visually analysed, of which of order half will turn out to be genuine.
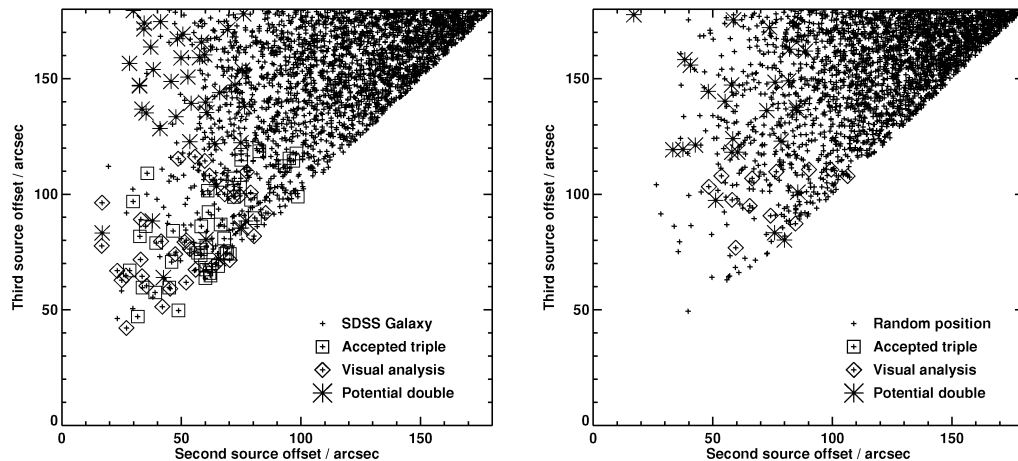
Figure 2. The positional offsets of the second and third nearest NVSS sources from those SDSS galaxies (left) and an equivalent number of random positions (right) which have three NVSS sources within 3 arcmin. As for Fig. 1, the criteria for the candidates to be accepted, rejected, classified as potential doubles (on the basis of their NVSS properties – further investigation with FIRST is then carried out to confirm or reject their double status), or referred to visual analysis are described in the text.

In addition to these, there is a clear excess of SDSS galaxies (compared to random) that have the two NVSS components each offset by 20–50 arcsec from the optical position. For these systems, the flux-weighted mean position of the two NVSS sources is often within 15 arcsec of the optical galaxy (indicated by the diamonds in the upper panel of Fig. 1). Candidate NVSS doubles are therefore selected to be sources with both NVSS components closer than 90 arcsec, a flux-weighted mean position closer than 15 arcsec, and the nearer component offset by more than whichever is smaller out of 15 arcsec and the offset of the second source minus 20 arcsec. These selection criteria are indicated by the lines on Fig. 1. The 90-arcsec limit is chosen because larger offsets are relatively unlikely and the contamination by random galaxies gets increasingly large beyond this. Even with this limit, there is still significant contamination, but the next step of comparison with FIRST helps to alleviate much of this.

All of these candidate doubles were cross-correlated with the FIRST catalogue. If these are true extended doubles then they may have a central FIRST component associated with a radio source core, and in addition they are likely to be missing flux in the FIRST data due to their extended nature; indeed they may well be undetected by FIRST. If they are not true doubles, but two individual NVSS sources, then it is likely that a single or double FIRST counterpart is present at each NVSS location, with little missing flux. The candidate doubles were thus classified into three categories as follows.

(a) Accepted doubles: sources were accepted as NVSS doubles if they either have a FIRST source within 3 arcsec of the optical position, or they satisfy the following three conditions (i) no detected FIRST component (i.e. all of the flux is resolved out by FIRST); (ii) both NVSS components lie within 60 arcsec of the SDSS position (larger sources may have additional NVSS components outside of the 3-arcmin limit, and so need to be checked visually); and (iii) the angle NVSS1-SDSS-NVSS2 greater than 135° (i.e. consistent with a double radio source with a bend of <45°).

(b) Rejected doubles: those sources with three or fewer FIRST components, all further than 15 arcsec from the optical galaxy, and with total flux greater than half of the sum of the two NVSS fluxes, were rejected.

(c) Uncertain cases: any sources not satisfying either of the above conditions were classified as uncertain, and referred for visual analysis.

The lower two plots of Fig. 1 show the results of this classification of candidate doubles for the SDSS sources and an equivalent number of random positions.

3.1.2 Candidate NVSS triples

Galaxies with three NVSS components within 3 arcmin could represent one of four possibilities: (i) a triple radio source associated with the galaxy; (ii) a double radio source associated with the galaxy, together with an unassociated NVSS source; (iii) a single radio source, with two unassociated sources (or an unassociated double source); (iv) three unassociated NVSS sources. It is the first two possibilities that are the concern for the multiple-source analysis.

Comparison between the SDSS galaxies and the random positions (Fig. 2) suggests that a source should be classified as a potential triple if all three components are within 120 arcsec, and one of the following three conditions is also satisfied: (i) the flux weighted mean position of all three components is within 15 arcsec of the optical galaxy position; (ii) the flux weighted mean position of the two more distant components is within 15 arcsec of the optical galaxy position (this for the case where these are the two outer lobes of a radio source, and the nearest component is a feature in the jet of one of the sources); (iii) the nearest component is within 15 arcsec of the optical galaxy, with the second and third components both within 90 arcsec and the angle NVSS2–NVSS1–NVSS3 greater than 135° (this is the case where the nearest component corresponds to the core of the triple: the offset and angle classification requirements distinguish this from a single-component source with two unassociated sources).

Galaxies which satisfied these constraints were investigated using FIRST to accept or reject obvious cases. Galaxies were accepted as triples if they possessed a FIRST source within 3 arcsec of the optical galaxy position. They were rejected if, as for the doubles, they had three or fewer FIRST components, all further than 15 arcsec from the optical galaxy, with total flux equal to at least half of the sum of the three NVSS fluxes. The remainder of the galaxies were referred

to visual analysis. Fig. 2 compares the results of this analysis for the SDSS galaxies and the random sample.

Galaxies that were neither classified as triples nor visually inspected were then investigated to see if they were associated with a double radio source. Each of the three NVSS pairs was checked using the double source analysis described above.

3.1.3 Candidates with four or more NVSS matches

Galaxies with four or more NVSS sources within 3 arcmin of the galaxy are likely either to be the host galaxy of a multiple-component radio source, or to lie close to one. No such cases were accepted without visual analysis. Visual analysis was carried out on all galaxies with five or more NVSS matches, as well as on galaxies with four NVSS matches where either the mean position or the flux-weighted mean position of the four NVSS sources was within 30 arcsec of the optical galaxy. All other galaxies were not considered to be quadrupoles, but were examined for potential triples and doubles using the criteria described above.

Overall, as a result of the multiple source analysis, 60 SDSS galaxies were accepted as NVSS multiple-component sources, compared to only 0.3 multiple-component sources predicted from the Monte Carlo simulations using random positions. This corresponds to less than 1 per cent contamination. A further 277 sources (0.13 per cent of the original sample) required visual analysis, of which 109 were ultimately accepted as genuine sources. This total of 169 accepted multi-NVSS-component sources corresponds to about 6 per cent of the entire SDSS radio source sample.

3.2 Single-component NVSS matches

For all galaxies not classified as multiple NVSS sources, Fig. 3 compares the distribution of offsets between SDSS galaxies and their nearest NVSS source with the result obtained for random positions. There is a clear excess of sources associated with SDSS galaxies at small radii. Because multiple sources have been removed and the analysis is restricted to brighter sources with well-defined positions, true sources with offsets larger than about 15 arcsec are not
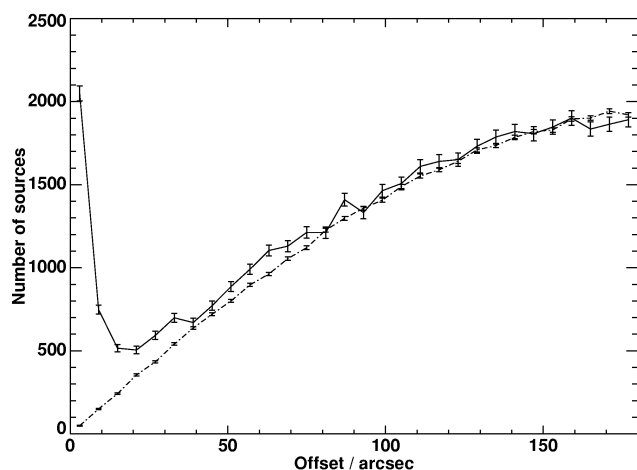
expected, but the excess is significant out to at least 100 arcsec. At these large radii the excess is not due to true associations, but rather is the result of the clustering of optical galaxies: on average there are more galaxies within ~100 arcsec of an optical galaxy than within the same distance of a random position, and hence there is an increased chance of finding an unassociated radio source. Note that in principle this effect could be accounted for by incorporating an appropriate correlation function into the positions of objects in the random catalogues; however, full knowledge of the environments of radio source hosts would be required to do this properly.

Integrating under the two curves of Fig. 3 out to a separation of 15 arcsec gives 2973 matches for the SDSS galaxies and 311 random matches, so the NVSS data alone would suffer from ≈10 per cent contamination if a 15 arcsec separation were adopted. This falls to ~6 per cent contamination at 10 arcsec, but at a cost of reducing the completeness by 10 per cent. The completeness can be improved by including information from the FIRST data. All SDSS galaxies with a single-component NVSS match within 30 arcsec are thus cross-correlated with the FIRST catalogue to determine the number of FIRST components within the 30-arcsec radius.

3.2.1 Sources with no FIRST matches

These sources are either variable radio-loud AGN which have faded between the NVSS and FIRST observations or they are extended radio sources which are resolved out of the FIRST data set. In either case they should be retained if they are associated with the optical galaxy. These NVSS sources are accepted as matches if they lie within 10 arcsec of the optical position. A total of 134 sources are retained in this way (compared to 8.7 random); this corresponds to approximately 5 per cent of the total radio source sample.

3.2.2 Sources with one FIRST match

For cases with one FIRST source within 30 arcsec, Fig. 4 compares the distribution of separations of the FIRST source and the SDSS galaxy with the result obtained for the random catalogue. An excess
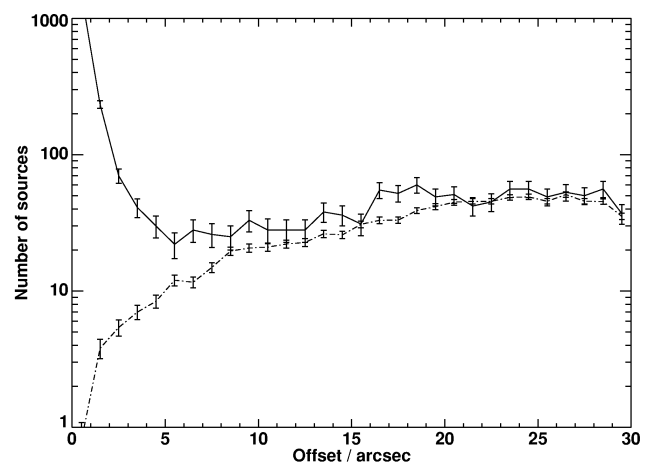

Figure 3. The positional offsets between SDSS galaxies and their nearest NVSS source (solid line) compared to the expectation derived from random positions (dot-dash line). There is a clear excess at small offsets, associated with true matches. Few if any true matches are expected above a separation of 15 arcsec; the excess at these radii is caused by the clustering of optical galaxies.

Figure 4. The positional offsets between SDSS galaxies and the FIRST source (solid line), for those SDSS galaxies with a single NVSS match of >5 mJy flux density within 30 arcsec and a single FIRST component associated with that. This is compared to the expectation derived from random positions (dot-dash line). The excess over the 10–30 arcsec range is likely associated with the clustering of optical galaxies; most of those with offsets less than 10 arcsec are likely to be true identifications.
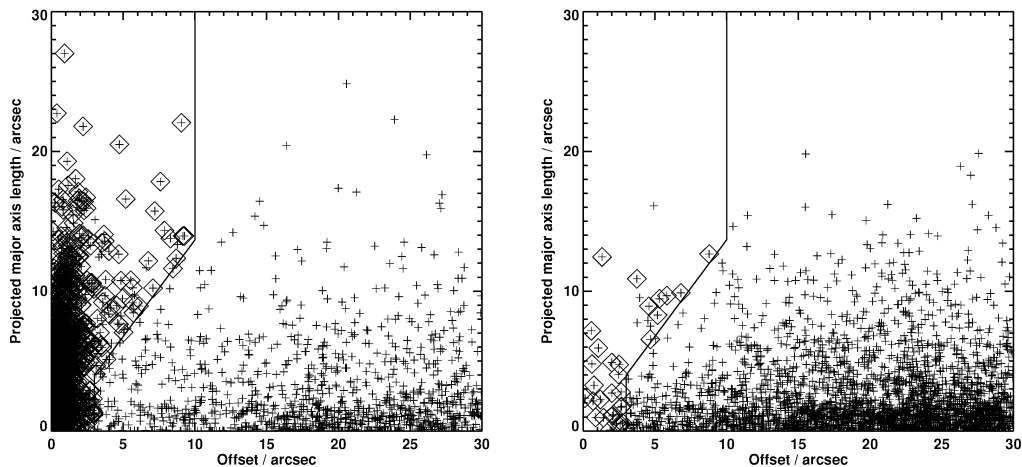
Figure 5. Left: for those SDSS galaxies with a single associated FIRST source, the projected major axis size of the FIRST source is plotted against its positional offset from the optical position. Right: the equivalent plot for the random positions. It is clear that much of the excess of SDSS–FIRST offsets of 3–10 arcsec is associated with extended FIRST sources. The solid lines indicate the allowed limits to the offset for a source to be considered a possible match, namely that the offset must be either less than 3 arcsec or be both between 3 and 10 arcsec and less than 75 per cent of the projected major axis length. The diamonds indicate the finally accepted sources: those with offsets less than 3 arcsec or which lie to the left of the solid line and are oriented within $30°$ of the offset vector (see text for full details).

of FIRST sources with respect to random is seen at all separations; at large separations this is the result of the clustering of optical galaxies, as discussed earlier. The excess becomes particularly pronounced at separations less than 10 arcsec, but at separations larger than ~ 3 arcsec the contamination of random sources is high. Within 3-arcsec separation, however, the fraction of false identifications is very low, $\lesssim 1$ per cent. This is lower than has been previously derived for simple SDSS-FIRST comparisons (e.g. Ivezić et al. 2002, who found a random contamination of about 9 per cent at 3-arcsec radius). This is because the present analysis is limited to galaxies with NVSS counterparts brighter than 5 mJy.

Given the low contamination rate, all FIRST radio sources with offsets below 3 arcsec can clearly be accepted as matches. If all sources between 3 and 10 arcsec were dropped, however, then the completeness would suffer. Fig. 5 compares the offset of the FIRST sources against their projected size along the offset direction, i.e. the product of the deconvolved major axis length and the cosine of the angle between the major axis and the offset vector. A significant fraction of the FIRST sources with offsets between 3 and 10 arcsec are found to be extended sources oriented close to the direction of the offset between the optical and radio position. Only a few of the random positions are associated with radio sources with these properties. The selection procedure was therefore refined to accept those FIRST sources which are either (i) within 3 arcsec, or (ii) offset less than 10 arcsec, oriented within $30°$ of the offset vector, and offset by less than 75 per cent of the projected major axis length of the source. These selection criteria are illustrated on Fig. 5. The addition of the 3–10 arcsec offset sources significantly reduces the incompleteness of the sample for only a small decrease in the reliability.

3.2.3 Sources with two FIRST matches

For galaxies with two FIRST matches, if the closer of the two matches is within 3 arcsec then the source is accepted under the assumption that it is either a single-component source with a nearby unassociated source, or the core of a core-jet source. There are 251 such SDSS galaxies (5.3 random). If neither FIRST source is within

3 arcsec, then it is possible that the two FIRST components are two lobes of the same extended radio source with no core. As discussed earlier, McMahon et al. (2002) found that in this case the two FIRST sources often have the following properties: (i) they have comparable flux densities; (ii) the flux-weighted mean position of the two sources is close to that of the optical galaxy; (iii) the sizes of the two sources are comparable (i.e. both are lobes, not a core and a lobe). None of these conditions on their own is sufficient to classify the source as a double without including a lot of false detections, but the Monte Carlo simulations show that the combination of the three can be quite powerful. Galaxies with two FIRST matches were accepted as double radio sources if the ratio of the radio source sizes, multiplied by the ratio of the radio source flux densities, multiplied by the offset in arcsec of the flux-weighted mean position, is less than 5. Fig. 6 shows the result of this analysis: 116 double sources are selected among SDSS galaxies, but only 1.2 for random positions, implying that the reliability is about 99 per cent.

It should be noted here that in cases where the galaxy is associated with a single FIRST component, and the other component (or components, for the cases with three or more matches discussed below) is genuinely unassociated, the NVSS flux will overestimate the radio luminosity owing to the contaminating source. However, only in very rare cases (i.e. a faint point source lying nearby a much brighter source) would such a correction be significant and these cases could not reliably be separated from core-jet type sources without visual analysis.

3.2.4 Sources with three FIRST matches

Galaxies for which there are three FIRST matches within 30 arcsec are accepted if any of the following three conditions are satisfied: (i) the nearest match is within 3 arcsec; (ii) any of the three pairs of sources satisfies the criteria to be accepted as a FIRST double source; (iii) the flux-weighted mean position of all three sources is within 3 arcsec of the optical galaxy position, with the angle subtended by the outer two sources relative to the middle one larger than
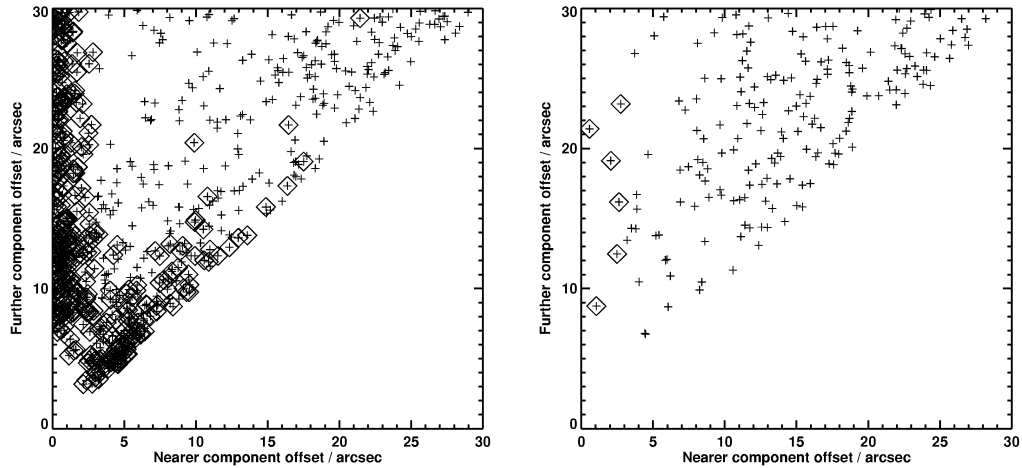
Figure 6. For those SDSS galaxies with a single NVSS match and two FIRST components associated with that, the left-hand panel shows the distribution of the positional offsets between the SDSS galaxies and the two FIRST sources. The right-hand panel shows the equivalent plot for random positions. Accepted singles and doubles (defined by the criteria described in the text) are indicated by diamonds.
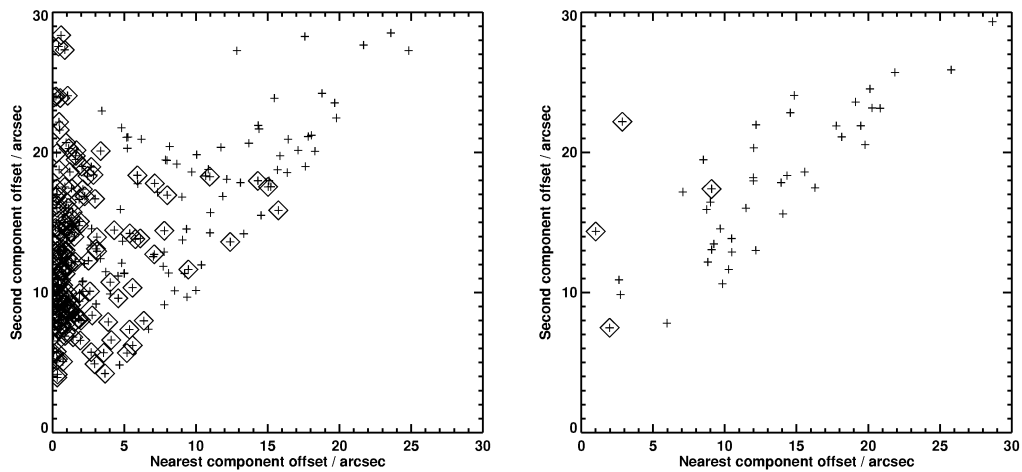

Figure 7. Left: the positional offsets between SDSS galaxies and the nearest two FIRST sources, for those SDSS galaxies with a single NVSS match within 30 arcsec, of >5 mJy flux density, and three FIRST components associated with that. Right: the equivalent plot for random positions. Accepted singles, doubles and triples (defined by the criteria described in the text) are indicated.

135° (i.e. the source looks like a straight(ish) triple source). Fig. 7 shows the results of this selection.

3.2.5 Sources with four or more FIRST matches

Automated classification of more than three sources cannot be carried out in an efficient and reliable way. For galaxies with four or more matches, the nearest three matches are analysed using the criteria for three-source matches to test whether they may be classified as triples, doubles or singles. All galaxies not accepted in this way are sent for visual analysis (a total of 23 optical galaxies or ~0.01 per cent of the SDSS sample).

3.3 Repeated matches

The final list of matches was examined to ensure that two different SDSS galaxies were not associated with the same NVSS source. This occurred on 24 occasions and these cases were all examined visually. In two cases, two SDSS galaxies were associated with

the same NVSS source and there was no FIRST counterpart. In a further 14 cases, two SDSS galaxies were associated with the same NVSS source which had a single FIRST counterpart which lay close enough to both galaxies. For these 16 objects, the nearer galaxy was accepted as the true match and the other galaxy was removed from the radio source catalogue. There were a further eight cases where it was found that two galaxies matched the same NVSS source but had distinct FIRST counterparts. In other words, both galaxies were genuine radio sources, but at the lower resolution of NVSS they had been convolved together. In these cases the flux density of the NVSS source was divided between the two galaxies according to the ratio of their integrated FIRST flux densities. If the galaxies still remained above the 5-mJy flux density limit, they were retained in the radio source catalogue.

3.4 Completeness and reliability of the matching procedure

The results of the cross-matching procedure are provided in Table 1. This table gives the number of SDSS galaxies accepted as radio

Table 1. Results of the analysis: the number of SDSS galaxies, and the number of random locations (scaled to the same total number of sources) falling into each category.

Source type		SDSS gals	Random
NVSS multiples	Accepted directly	60	0.3
NVSS multiples	Visual analysis	(277)	(92.1)
	of which confirmed	109	
NVSS singles	0 FIRST matches	134	8.7
	1 FIRST match	1805	12.3
	2 FIRST matches	367	6.5
	3 FIRST matches	163	1.4
	4+, confirmed	57	0.9
	4+, visual analysis	(23)	(4.5)
	of which confirmed	17	
Total	Confirmed	2712	30.1

Figure 8. A histogram of the FIRST to NVSS flux density ratios of the final radio source sample. Sources without a detected central FIRST component (either because they are resolved out, or because they are extended multicomponent FIRST sources) are included in the left-most bin.

sources compared to the number of cases accepted from the same number of random positions, for each different radio source type. It therefore provides a direct measure of the reliability of each of the criteria defined above. Overall, assuming visual analysis to be 100 per cent reliable, only 30.1 false identifications are expected amongst the final sample of 2712 radio sources. This corresponds to an overall reliability of 98.9 per cent. The most unreliable part of the sample selection is for NVSS sources without a FIRST counterpart. Of these, 6 per cent will be false identifications. This is unavoidable. If sources with no FIRST counterpart are excluded, this reduces the completeness and strongly biases the derived radio source sample by removing 5 per cent of the more extended sources.

The completeness of the sample is more difficult to estimate than the reliability, because the true number of matches expected is unknown. However, various estimates can be made. For galaxies with multiple NVSS components, a comparison of the number of candidate NVSS doubles in the SDSS and random samples with the numbers accepted suggests that the completeness is close to 90 per cent. For the single NVSS component sources, Fig. 3 shows that there were 2973 SDSS galaxies with an NVSS source within 15 arcsec, compared to only 311 random galaxies. Assuming that this excess is entirely owing to genuine sources and that all true matches lie within 15 arcsec, 2662 genuine single-component NVSS sources are expected. Table 1 indicates that 2543 single-component sources were actually found by the adopted selection procedures, of which about 30 will be false detections. An estimate of the completeness is then $(2543-30)/2662 = 94.4$ per cent. Note that this value is conservative because a fraction of the excess matches are likely to be associated with companion galaxies, and so 2662 is an overestimate of the true number of expected matches. Therefore, the overall completeness of the sample likely exceeds 95 per cent.

The values quoted for completeness and reliability are for all types of radio source. There will be a small (but unavoidable) bias against extended sources: the completeness for the single-component FIRST sources approaches 100 per cent, while that of multi-NVSS-component sources is around 90 per cent. Note that completeness estimates from previous cross-correlations with the FIRST catalogue have not taken into account the sources missed because sources with radio-optical offsets greater than 3 arcsec are excluded ($\sim$3 per cent of our final source catalogue) as are sources that are completely resolved out by FIRST (5 per cent). These samples will also miss a fraction of the extended NVSS sources (6 per cent) and the multicomponent FIRST sources (6 per cent). These omissions have a severe effect on the completeness of any radio
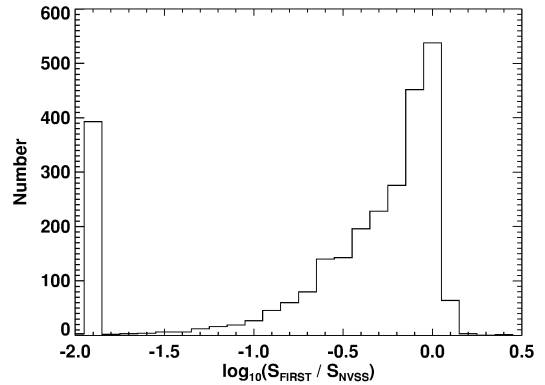
sample derived for the SDSS spectroscopic sample using the FIRST survey alone. The radio luminosities of many sources would also be underestimated using FIRST alone: the distribution of FIRST to NVSS flux density ratios for the final sample of sources is plotted in Fig. 8, and shows a long tail to low values. Note, however, that all of these effects are somewhat less important when dealing with the complete imaging catalogue of SDSS, for which the galaxies typically lie at higher redshifts.

3.5 The final radio source sample

Details of the final SDSS radio sample of 2712 sources are given in Table 2. This table provides the identification details of each source so that they can be matched against either the original spectra or against the catalogues of derived optical properties released by Brinchmann et al. (2004a). Also provided are the RA and Dec. of each source, the host galaxy redshift, the integrated NVSS flux density and, where there is a central FIRST counterpart, the integrated flux density, radio size and offset from the optical galaxy of the central FIRST component. Each radio source is also given a classification to identify its radio properties. Class 1 sources are single-component NVSS sources with a single FIRST counterpart. Class 2 sources have a single NVSS match which is resolved into multiple components by FIRST. Class 3 sources have a single-component NVSS source, but no FIRST counterpart. Class 4 sources have multiple NVSS components. The final column of the table classifies each radio source as a star-forming galaxy or a radio-loud AGN, according to the criteria described in Section 4.

4 DEFINITION OF THE RADIO-LOUD AGN SAMPLE

The sample of radio-emitting galaxies contains both radio-loud AGN and a population of star-forming galaxies. The latter emit at radio wavelengths mostly as a result of the synchrotron emission of particles accelerated in supernova shocks, and their radio luminosity is therefore roughly correlated with their star formation rate: a 1.4-GHz radio luminosity of 10^{22} W Hz^{-1} corresponds to a star formation rate of order 5 M$_\odot$ yr^{-1} (e.g. Condon 1992 and references therein; Carilli 2001). In order to investigate the host galaxies of these two populations, it is first necessary to separate the radio-loud AGN from the star-forming galaxies.

Table 2. Properties of the 2712 SDSS radio galaxies. (Only the first 30 sources are listed here: the full table is available in the online version of this article in the Supplementary Material section.) The first three columns give the identification of the targeted galaxies through their plate and fibre IDs and the date of the observations. Columns 4–6 give the RA, Dec. and redshift of the galaxies. Column 7 gives the integrated flux density of the source as measured using the NVSS. Column 8 provides the radio classification of the source: class 1 are single-component NVSS sources with a single FIRST match; class 2 are single-component NVSS sources resolved into multiple components by FIRST; class 3 are single-component NVSS source without a FIRST counterpart; class 4 sources are those which have multiple NVSS components. Where a galaxy has a central FIRST component, the integrated flux density, offset from the optical galaxy, and radio size of that central FIRST component are given in columns 9–11. The final column provides the classification of the source as either a radio-loud AGN or a star-forming galaxy, according to the criteria described in Section 4. Other properties of the host galaxy, such as stellar mass, [O III] emission-line luminosity, $D_n(4000)$, etc can be obtained from the data released by Brinchmann et al. (2004a), by cross-comparing the host galaxy identifiers.

Plate ID	Julian date	Fibre ID	RA (J2000) (°)	Dec. (°)	z	S_{NVSS} 1.4 GHz (Jy)	Radio class	S_{FIRST} 1.4 GHz (Jy)	Offset (arcsec)	Radio size (arcsec)	Source type
266	51630	25	146.95610	−0.3423	0.1347	0.0963	1	0.1010	1.26	4.64	Radio-loud AGN
266	51630	90	146.14360	−0.7416	0.2039	0.0068	1	0.0025	0.46	5.88	Radio-loud AGN
266	51630	119	146.73711	−0.2522	0.1305	0.0075	1	0.0043	0.51	2.39	Radio-loud AGN
266	51630	141	146.37379	−0.3684	0.0529	0.0104	1	0.0010	2.02	0.27	Star forming
266	51630	223	145.60120	−0.0014	0.1459	0.0054	1	0.0049	0.44	0.00	Star forming
266	51630	506	146.46300	0.6387	0.0303	0.0052	1	0.0028	2.10	6.24	Star forming
266	51630	517	146.37360	0.2555	0.1292	0.0275	1	0.0269	0.33	1.77	Radio-loud AGN
266	51630	543	146.80679	0.6656	0.0201	0.0180	1	0.0131	0.78	10.89	Radio-loud AGN
266	51630	545	146.79910	0.7027	0.0305	0.0063	1	0.0045	2.73	13.71	Star forming
266	51630	572	146.78149	0.7380	0.2618	0.0489	1	0.0094	0.77	5.71	Radio-loud AGN
266	51630	613	147.08051	0.7880	0.2111	0.0081	1	0.0078	0.68	0.00	Radio-loud AGN
267	51608	34	149.16991	−0.0233	0.1392	0.1661	4	0.0022	0.27	4.37	Radio-loud AGN
267	51608	47	148.43250	−1.0264	0.1103	0.0092	1	0.0111	0.06	1.45	Star forming
267	51608	97	148.23770	−0.7920	0.0898	0.0207	1	0.0169	0.43	2.69	Radio-loud AGN
267	51608	205	147.70860	−0.8878	0.2715	0.0558	1	0.0151	0.67	6.88	Radio-loud AGN
267	51608	260	147.42830	−0.8401	0.0809	0.1671	1	0.0115	0.40	0.00	Radio-loud AGN
267	51608	297	147.20770	−1.1859	0.1282	0.0129	1	0.0124	0.07	1.26	Radio-loud AGN
267	51608	497	148.23340	0.3577	0.2550	0.0570	1	0.0208	2.26	8.44	Radio-loud AGN
267	51608	512	148.37680	0.4487	0.0797	0.0118	1	0.0128	0.22	2.99	Radio-loud AGN
268	51633	38	150.47060	−0.1252	0.0329	0.0364	1	0.0260	0.45	3.68	Radio-loud AGN
268	51633	271	149.28870	0.0092	0.1255	0.0108	1	0.0049	0.69	4.57	Radio-loud AGN
268	51633	394	148.95151	0.5569	0.0800	0.0117	1	0.0085	0.05	1.37	Radio-loud AGN
268	51633	433	149.33859	0.7065	0.0874	0.0055	1	0.0038	1.39	2.58	Star forming
268	51633	461	149.35471	0.7309	0.0869	0.0080	1	0.0066	1.24	5.78	Star forming
268	51633	479	149.39481	0.2386	0.1602	0.0229	1	0.0092	0.64	2.67	Radio-loud AGN
268	51633	489	149.64740	0.7428	0.0648	0.0065	1	0.0064	0.28	2.27	Star forming
269	51910	59	151.36320	−0.8746	0.2057	0.0051	1	0.0010	0.60	0.00	Radio-loud AGN
269	51910	171	151.33971	0.0886	0.1793	0.0087	1	0.0080	0.38	0.00	Radio-loud AGN
269	51910	257	150.47040	−0.8781	0.1364	0.1507	4	–	–	–	Radio-loud AGN
269	51910	289	149.91280	−1.2480	0.1375	0.0114	1	0.0111	0.29	1.39	Radio-loud AGN
...	...	...	...	...	...	...	...	...	...	...	...

Star-forming galaxies and AGN are often separated using optical emission-line properties. Sadler et al. (2002) used a visual emission-line classification in their study of radio sources in the 2dFGRS: radio-emitting galaxies without detectable emission lines were classified as radio-loud AGN. Kauffmann et al. (2003c) used the location of a galaxy in the [O III] 5007/Hβ versus [N II] 6583 / Hα emission-line diagnostic diagram (Baldwin, Phillips & Terlevich 1981; hereafter BPT) to separate optical AGN from normal star-forming galaxies. A key result of the Kauffmann et al. study was that a significant fraction of emission-line selected AGN also have associated star formation. This result means that optical line ratio diagnostics should not be used to identify radio-loud AGN, because star formation activity in galaxies with a radio-quiet active nucleus would give rise to radio emission (and hence a radio-loud classification). In addition, for galaxies which do contain a genuine radio-loud AGN, the radio luminosity associated with the active nucleus will be overestimated if there is a significant contribution of star formation to the radio emission.

Machalski & Condon (1999) studied radio galaxies in the LCRS and used FIR to radio flux density ratios and FIR spectral indices to separate the radio-loud AGN and star-forming populations. The FIR radio correlation for star-forming galaxies (e.g. Yun, Reddy & Condon 2001) could also be used to correct for the contribution of star formation to the radio luminosities of these systems. This is perhaps the ideal method, but unfortunately the Infrared Astronomical Satellite (*IRAS*) Faint Source Catalogue is not quite deep enough to allow this to be used for the SDSS galaxies in this paper.[2] A variety of alternative methods were therefore considered, and a procedure

[2] In fact, the *IRAS* Faint Source Catalogue is deep enough that the *majority* of star-forming galaxies with 1.4-GHz radio flux densities of 5 mJy are detected (and lie as expected on the FIR radio correlation), plus a few of the AGN, but the observations are not deep enough that *all* star-forming galaxies are detected. The *IRAS* data cannot therefore be used as a discriminant between the two subclasses, nor to correct for any star formation contribution to the radio emission of the AGN.

based on the location of a galaxy in the plane of $D_n(4000)$ versus $L_{1.4\,GHz}/M_*$ was adopted. The $L_{1.4\,GHz}/M_*$ ratio provides the radio luminosity per stellar mass of the galaxy and $D_n(4000)$ is a fairly accurate indicator of mean stellar age for ages below about a Gyr (at higher ages it is also sensitive to metallicity; cf. Kauffmann et al. 2003b). Thus, star-forming galaxies would be expected to occupy a well-defined locus in this plane, while radio-loud AGN would be offset to higher radio luminosities. This is demonstrated in the first two panels of Fig. 9.

The top panel of Fig. 9 shows $D_n(4000)$ versus $L_{1.4\,GHz}/M_*$ for radio-emitting galaxies that are classified as star-forming galaxies using the [O III] 5007/Hβ versus [N II] 6583/Hα emission-line diagnostic diagram. The criteria of Kauffmann et al. (2003c) have been adopted and only galaxies with redshifts in the range $0.03 \leqslant z \leqslant 0.10$ have been plotted; the lowest redshifts are excluded because aperture corrections are substantial, whilst beyond $z = 0.1$ the sensitivity to emission lines is low, hampering classification by emission-line diagnostics. Radio luminosities have been calculated from the fluxes assuming a radio spectral index of 0.7.

Overlaid on this are theoretical predictions, derived using the Bruzual & Charlot (2003) stellar synthesis models, for the location of galaxies with different star formation histories. For these models, the radio luminosities have been calculated using the prescription of Hopkins et al. (2001): $L_{1.4\,GHz} = 1.8 \times 10^{21}$ (SFR/M$_\odot$) W Hz^{-1}, where SFR is the average star formation rate in the past 10^8 yr. Three of the models are for galaxies with exponentially decaying star formation rates, of characteristic timescales 1, 3 and 5 Gyr; the tracks indicate how these galaxies move across this plane as they age. A fourth model shows the track for a galaxy with a constant star formation rate. Two further models consider an old (10 Gyr) galaxy which has undergone a recent burst of star formation (10^7 and 10^8 yr ago), as might be the case for a merger-triggered event. Here, the loci of the tracks show what happens if different fractions of the total galaxy mass are converted into stars in the burst. These theoretical tracks largely cover the location of the data points.

The middle left-hand panel of Fig. 9 shows the same plot, but now includes all radio-emitting galaxies in this redshift range. The different colours represent different galaxy classifications based upon their locations in the BPT diagram (black, star-forming galaxy; red, composite systems with both star formation and an AGN; orange, Seyfert AGN; green, LINER AGN; purple, no emission lines). A significant number of the objects classified as AGN based on their emission-line ratios overlap the star-forming population in this plane. This is interpreted as meaning that these are radio-quiet AGN whose radio emission is due to star formation – the problem identified earlier. The dotted line on this plot shows the 3-Gyr exponential star formation model from the top panel. The solid line, 0.225 above this in $D_n(4000)$, is the proposed division between radio-loud AGN (above the line, plotted as diamonds) and star-forming galaxies (below the line, plotted as crosses). This cut-off value was chosen to be most consistent with other methods that could have been adopted for AGN–starburst separation, as illustrated in the later panels. Using this cut-off, 2215 radio sources are classified as radio-loud AGN, and 497 as star forming. Note that the plots only show the subset of these at redshifts with $0.03 \leqslant z \leqslant 0.1$, to avoid overcrowding the plot and to allow a comparison with emission-line diagnostic methods; the higher redshift sources fill out more of the plane at larger values of $L_{1.4\,GHz}/M_*$, and confirm that the location of the proposed cut at those values is appropriate.

The middle right-hand panel shows the BPT emission-line diagnostic diagram. It can be seen that the AGN–starburst separation defined above (i.e. diamonds versus crosses) also makes good sense

in this plot: (i) the 'composite' galaxies that lie close to the star-forming galaxy locus are largely classified as starbursts, whilst those nearer to the AGN locus are predominantly classified as radio-loud AGN; (ii) almost all of the LINERS are classified as radio-loud AGN; (iii) the Seyferts close to the LINER region are mostly classified as radio-loud, whilst those with lower [N II] 6583/Hα ratios are a mixture of the two classes; (iv) the three star-forming galaxies now classified as radio-loud AGN all lie near the boundary with composites.

The lower left-hand panel shows the Hα/Hβ line ratio as a function of galaxy stellar mass. The Hα/Hβ line ratio is an approximate measure of dust reddening; the dotted line shows the expected value for zero reddening. Star-forming galaxies form a tight relation between these parameters, with more massive galaxies being more heavily reddened (cf. fig. 6 of Brinchmann et al. 2004b). Radio-loud AGN deviate from this locus, in the sense of having less reddening (due to less star formation and hence less dust) at a given stellar mass; this diagram indicates that the classification division adopted for $D_n(4000)$ versus $L_{1.4\,GHz}/M_*$ works well.

The final panel shows the distribution of the galaxies in the $L_{[O\,III]5007}$ versus $L_{1.4\,GHz}$ plane. This relation was considered as a way to separate radio-loud AGN and star-forming galaxies; indeed, it can be seen that for the LINERS and the galaxies without emission lines the division agrees very well with that adopted. However, many of the Seyferts and composites lie on the relation defined by the star-forming galaxies in this plane, but are considerably offset from the star-forming locus in all of the other plots. It is for this reason that the final classification was not based upon this relation.

These plots demonstrate the reliability of the AGN–starburst separation using the $D_n(4000)$ versus $L_{1.4\,GHz}/M_*$ relation: through comparison of the locations of galaxies on different diagnostics, it is estimated that $\lesssim 1$ per cent of objects will have been misclassified. The $D_n(4000)$ versus $L_{1.4\,GHz}/M_*$ relation was also used to estimate and to correct for the star formation contribution to the radio luminosity of galaxies classified as radio-loud AGN: for each of these galaxies the 'star formation' radio luminosity corresponding its 4000-Å break strength, as estimated by the 3-Gyr exponential star formation track (the dotted line in the middle left-hand panel), was subtracted to obtain a corrected AGN radio luminosity. In no case was this correction larger than 15 per cent.

The radio-loud AGN in the sample exhibit a variety of optical properties; some are classified as optical AGN based upon their emission lines while others are optically inactive. Fig. 10 shows the cumulative fractions of the different radio source types as a function of redshift. Out to redshifts $z \sim 0.1$, the relative numbers of radio-loud AGN with and without emission lines are roughly similar. At higher redshifts the proportion of emission-line AGN decreases rapidly; this is because emission lines such as [O III] 5007 become increasing difficult to detect at higher redshift (only lines brighter than $\sim 10^{5.8}$ L$_\odot$ can be detected at $z = 0.1$), both because of the increased distance and because the larger physical size of the spectroscopic fibres means that a larger fraction of starlight from the host galaxy is included. This makes it more difficult to pick out the weaker nuclear lines.

5 THE LOCAL RADIO LUMINOSITY FUNCTION

The local radio luminosity function was derived for both radio-loud AGN and radio-emitting star-forming galaxies out to redshift 0.3. These were calculated in the standard way using the $1/V_{max}$ method (Schmidt 1968; Condon 1989), where V_{max} was calculated
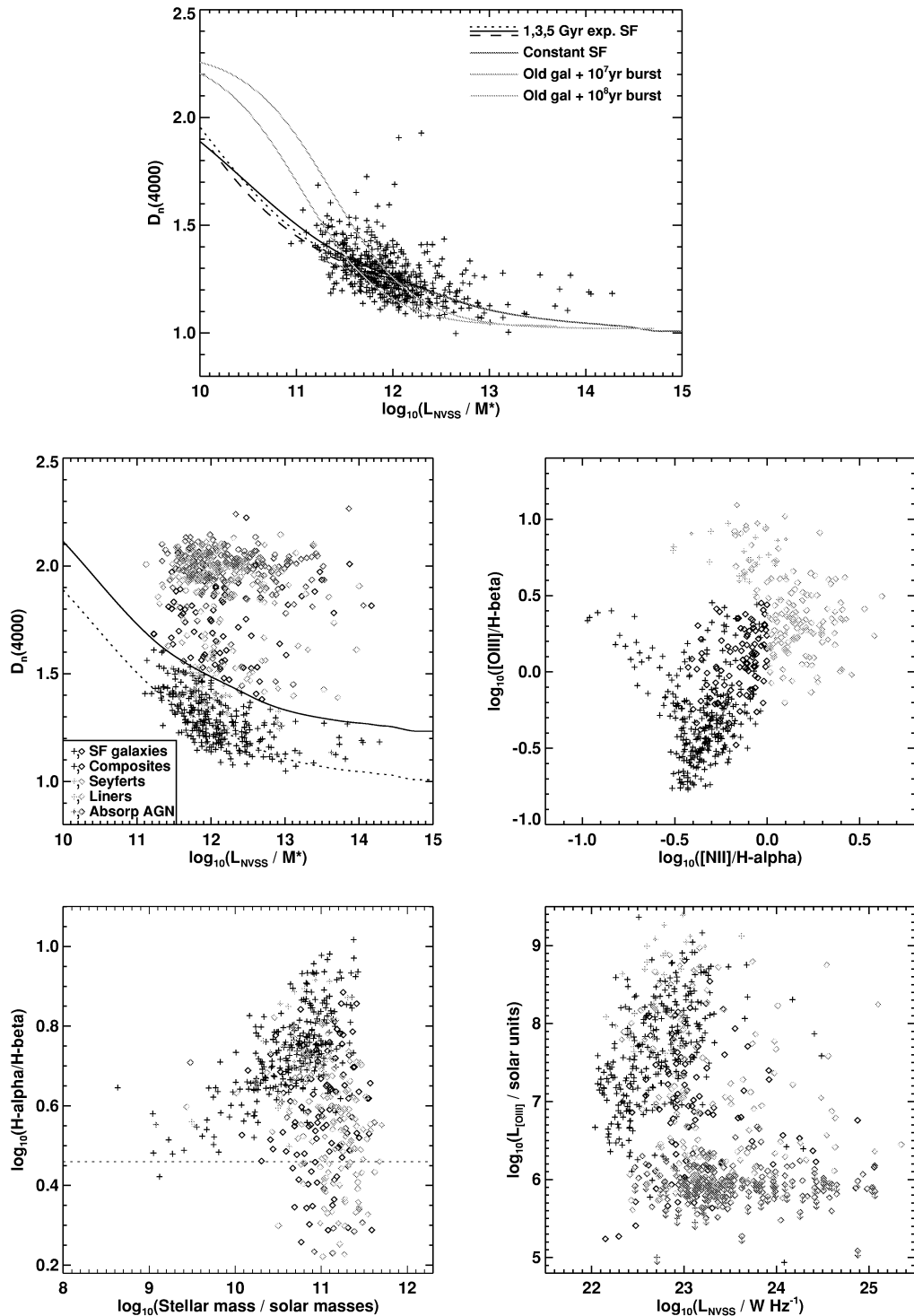
Figure 9. The separation of radio-loud AGN from starbursting galaxies in SDSS. The top panel shows $D_n(4000)$ versus $L_{1.4\,GHz}/M_*$ for radio-emitting galaxies (brighter than 2.5 mJy) classified as star forming in the [O III] 5007/Hβ versus [N II] 6583/Hα emission-line diagnostic diagram using the criteria of Kauffmann et al. (2003c). Overlaid on this are theoretical predictions for galaxies with different star formation histories, as derived using the Bruzual & Charlot (2003) stellar synthesis models (see text for details). These models are able to explain the locus of the star-forming galaxies. The middle left-hand panel shows this same plot for all radio-emitting galaxies brighter than 5 mJy. The different colours represent different galaxy classifications based upon their locations in the emission-line diagnostic diagram. The dotted line is the 3 Gyr exponentially decaying star formation track of the top panel and the solid line, 0.225 above this in $D_n(4000)$, is the proposed division between radio-loud AGN (indicated by diamonds) and galaxies whose radio emission is dominated by star formation (crosses). The colours and symbols are identical on the following three panels. The middle right-hand panel shows the emission-line diagnostic diagram for these galaxies, the lower left-hand panel shows the Hα/Hβ ratio versus stellar mass (the dotted line indicates the value for zero reddening), and the lower right-hand panel shows the distribution of the galaxies in the $L_{[O\,III]\,5007}$ versus $L_{1.4\,GHz}$ plane. These final three plots show that the AGN–starburst classification derived works very well.
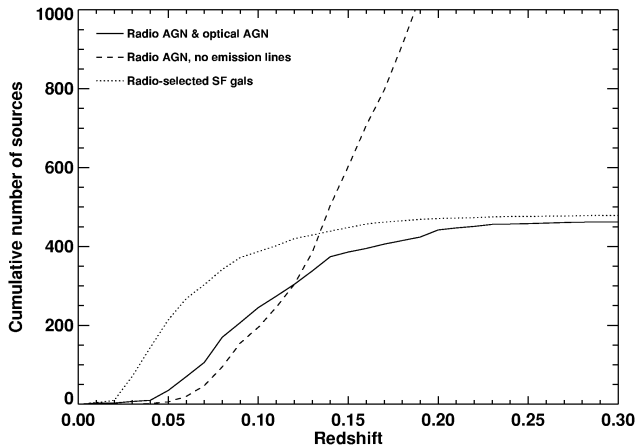
Figure 10. The cumulative number, as a function of redshift, of radio-selected star-forming galaxies, optically passive radio-loud AGN and radio-loud AGN with optical AGN characteristics, in the SDSS sample. [The line for AGN with emission lines continues to rise to nearly 1800 by $z = 0.3$].

using the upper and lower redshift limits determined by the joint radio and optical selection criteria, namely a radio cut-off of 5 mJy and optical cut-offs of $14.5 < r < 17.77$. An accurate calculation of the exact area of sky within the overlap region of the SDSS DR2 and the FIRST survey is not simple. The absolute normalization of the derived radio luminosity function has thus been set by normalizing the total radio luminosity function to match that derived for the

2dFGRS by Sadler et al. (2002) over the radio luminosity range 10^{23}–$10^{24.5}$ W Hz^{-1}, where the errors on the two luminosity function determinations are both small. Note that no correction has been made for incompleteness or misidentification in the radio samples but, as discussed above, it is expected that this will be relatively small.

The radio luminosity functions are tabulated in Table 3. The uncertainties quoted on the luminosity function determination are the statistical Poissonian errors only; these have become so small for the SDSS sample at some luminosities that systematic errors are likely to dominate. One important source of systematic error will be cosmic variance. Another is the separation of AGN and star-forming galaxies: for the highest luminosity bin of the star-forming galaxies and the lowest luminosity bin of the AGN, this systematic error is likely to be comparable to or larger than the Poissonian uncertainties.

The radio luminosity functions are displayed in Fig. 11, along with the results of Sadler et al. (2002) for the 2dFGRS and Machalski & Godlowski (2000) for the LCRS (both corrected to the cosmology adopted in this paper; note that these determinations are not corrected for incompleteness either). The luminosity function of radio-loud AGN generally agrees well with these previous analyses, although with notably smaller errors. The apparent small mismatches between the Sadler et al. results and those of this paper at $10^{24.5}$ and $10^{25.5}$ W Hz^{-1} are likely to be due to cosmic variance.

The luminosity function of star-forming galaxies has similar shape to previous measurements, but with slightly higher space densities at high luminosities ($L_{1.4\,\mathrm{GHz}} > 10^{23}$ W Hz^{-1}). There are three possible differences between the analyses which could account for this. First, the different optical magnitude limits of the different

Table 3. The local radio luminosity function at 1.4 GHz, derived separately for radio-loud AGN and star-forming galaxies.

| $\log_{10} L_{1.4\,\mathrm{GHz}}$ (W Hz^{-1})	All radio sources		Radio-loud AGN		Star-forming galaxies	
	N	$\log_{10}\rho$ $(\log_{10} L)^{-1}$ Mpc^{-3}	N	$\log_{10}\rho$ $(\log_{10} L)^{-1}$ Mpc^{-3}	N	$\log_{10}\rho$ $(\log_{10} L)^{-1}$ Mpc^{-3}
21.60–21.90	10	$-2.92^{+0.13}_{-0.18}$			10	$-2.92^{+0.13}_{-0.18}$
21.90–22.20	64	$-3.19^{+0.05}_{-0.06}$			64	$-3.20^{+0.05}_{-0.06}$
22.20–22.50	105	$-3.39^{+0.05}_{-0.05}$	15	$-4.23^{+0.11}_{-0.15}$	90	$-3.46^{+0.05}_{-0.06}$
22.50–22.80	132	$-3.79^{+0.04}_{-0.04}$	43	$-4.27^{+0.07}_{-0.08}$	89	$-3.96^{+0.05}_{-0.05}$
22.80–23.10	195	$-4.04^{+0.03}_{-0.04}$	115	$-4.29^{+0.04}_{-0.05}$	80	$-4.41^{+0.06}_{-0.07}$
23.10–23.40	219	$-4.44^{+0.03}_{-0.03}$	157	$-4.59^{+0.03}_{-0.04}$	62	$-4.99^{+0.05}_{-0.06}$
23.40–23.70	335	$-4.68^{+0.02}_{-0.03}$	291	$-4.75^{+0.03}_{-0.03}$	44	$-5.55^{+0.06}_{-0.07}$
23.70–24.00	459	$-4.93^{+0.02}_{-0.02}$	448	$-4.94^{+0.02}_{-0.02}$	11	$-6.44^{+0.12}_{-0.17}$
24.00–24.30	389	$-5.12^{+0.05}_{-0.05}$	389	$-5.12^{+0.02}_{-0.02}$		
24.30–24.60	303	$-5.33^{+0.03}_{-0.04}$	303	$-5.33^{+0.03}_{-0.03}$		
24.60–24.90	184	$-5.56^{+0.04}_{-0.04}$	181	$-5.56^{+0.04}_{-0.04}$		
24.90–25.20	108	$-5.81^{+0.05}_{-0.05}$	108	$-5.81^{+0.05}_{-0.05}$		
25.20–25.50	35	$-6.28^{+0.09}_{-0.11}$	35	$-6.28^{+0.09}_{-0.11}$		
25.50–25.80	8	$-6.87^{+0.15}_{-0.23}$	8	$-6.87^{+0.15}_{-0.23}$		
25.80–26.10	2	$-7.68^{+0.23}_{-0.53}$	2	$-7.68^{+0.23}_{-0.53}$		
26.10–26.40	1	$-8.00^{+0.30}_{-1.00}$	1	$-8.00^{+0.30}_{-1.00}$		
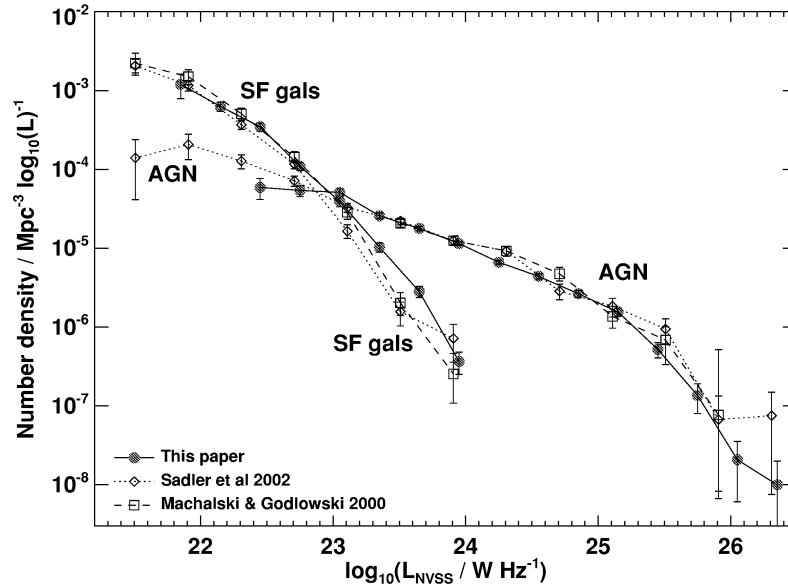
Figure 11. The local radio luminosity function at 1.4 GHz derived separately for radio-loud AGN and star-forming galaxies. Filled points connected by solid lines indicate the data derived in this paper, using the SDSS. No correction has been made for incompleteness or misidentification, but such effects are small. For comparison, the results of Sadler et al. (2002) using the 2dFGRS, and those of Machalski & Godlowski (2000) using the LCRS are also plotted. The AGN results are in excellent agreement between the different samples. The results for star-forming galaxies are in broad agreement but with small differences in normalization at the larger luminosities.

surveys may influence the population of radio star-forming galaxies studied. Secondly, the combined FIRST-NVSS radio-optical cross-correlation method adopted here will lead to a more complete sample, particularly for low-redshift star-forming galaxies with extended radio emission. Third, the disparity might arise from the contrasting ways in which different analyses treat radio-quiet AGN with associated star formation activity, for which the radio emission is due to the star formation. The technique used in the current paper for separating the star-forming and AGN populations would classify such objects as star-forming galaxies, but in emission-line ratio classifications (as used, for example, by Sadler et al.) they might be classified as AGN. This would lead to previous studies estimating a lower space density of star-forming galaxies, particularly at the highest radio luminosities. Note that if star formation dominates the radio and FIR emission of these radio-quiet AGN, then these objects would be expected to lie on the FIR radio correlation for star-forming galaxies, despite being classified (by emission line means) as AGN. In this respect it is interesting to consider fig. 10 of Sadler et al. which shows the FIR radio relation for the objects in their sample; many of the objects which lie on the FIR radio relation for star-forming galaxies, but which have radio luminosities $L_{1.4\,\mathrm{GHz}} > 10^{23}\,\mathrm{W\,Hz^{-1}}$, are indeed classified as AGN. If just some of these objects are truly radio quiet AGN, with radio emission due to associated star formation activity, they could easily account for the small difference between the luminosity function determinations.

It is instructive to compare the radio luminosity function for star-forming galaxies with that derived at FIR wavelengths. Star-forming galaxies show a tight correlation between their radio and FIR luminosities, which Yun et al. (2001) showed for the range of luminosities probed in the current study to be indistinguishable from a linear relation: $L_{1.4\,\mathrm{GHz}}/\mathrm{W\,Hz^{-1}} = 10^{11.95}\,L_{60\,\mu\mathrm{m}}/\mathrm{L_\odot}$. The local FIR luminosity function need only be adjusted by this factor to estimate the local radio luminosity function.

Takeuchi, Yoshikawa & Ishii (2003) derived the local FIR luminosity function using the *IRAS* Point Source Catalogue redshift survey (PSCz; Saunders et al. 2000). They fitted the data with an analytic function of the form suggested by Sandage, Tammann & Yahil (1979), namely

$$\phi(L) = \phi_* \left(\frac{L}{L_*}\right)^{1-\alpha} \exp\left(\frac{-1}{2\sigma^2}\left[\log\left(1 + \frac{L}{L_*}\right)\right]^2\right)$$

with $\alpha = 1.23 \pm 0.04$, $\phi_* = (2.60 \pm 0.30) \times 10^{-2}\,h^3\,\mathrm{Mpc^{-3}}$, $\sigma = 0.724 \pm 0.01$ and a characteristic luminosity of $L_* = (4.34 \pm 0.87) \times 10^8\,h^{-2}\,\mathrm{L_\odot}$ (where h is H_0 in units of $100\,\mathrm{km\,s^{-1}\,Mpc^{-1}}$). Converting the characteristic luminosity by the factor given, the equivalent local radio luminosity function is shown as the solid line in Fig. 12. This provides a good match to the data at high radio luminosities, supporting the division adopted between AGN and star-forming galaxies. The match is less than perfect at lower luminosities, however. The luminosity range covered by the radio observations is not sufficient constrain the parameters for a fit of the above form using the radio data, but the dotted and dashed lines show the effect of doubling the characteristic luminosity or setting the faint end slope α to unity (with corresponding changes in ϕ_*); these provide a much better fit to the data. However, these represent much larger changes than are allowed by the errors on the fitted FIR parameters or on the radio to FIR conversion.

The difference between the radio and FIR luminosity functions means that the observed radio to FIR correlation stops being a linear relation at low luminosities. This has been suggested before in terms of a steepening of the relation below $L_{60\,\mu\mathrm{m}} \sim 10^9\,\mathrm{L_\odot}$ (cf. Yun et al. 2001 and references therein) but questions have been raised as to whether the previous studies may be affected by selection biases in the samples under study. Here it is shown that the difference is also present in the luminosity functions. The difference occurs for the lowest luminosity sources, which are generally at the lowest redshifts and therefore may have larger angular sizes, in which case it may be caused by photometric errors due to aperture effects. This is unlikely to be the case, however. The NVSS is sensitive to emission
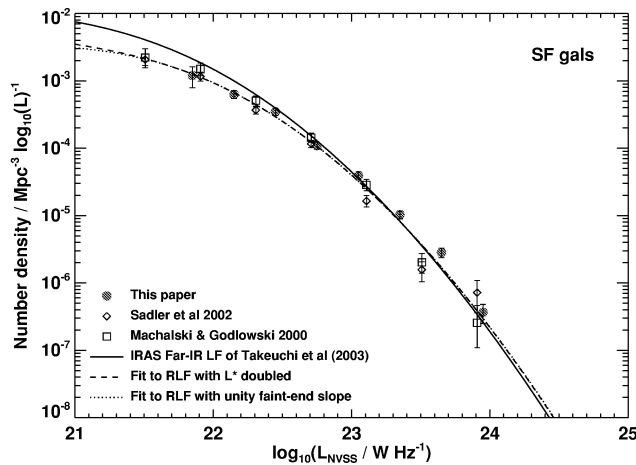
Figure 12. The local radio luminosity function at 1.4 GHz derived for star-forming galaxies; symbols are as in Fig. 11. The solid line represents the FIR luminosity function as derived by Takeuchi et al. (2003) using the *IRAS* PSCz survey, converted to the radio band using the radio to FIR conversion of Yun et al. (2001). The dotted and dashed lines show that improved fits at low luminosities can be obtained by, respectively, doubling the characteristic luminosity or setting the faint end slope to unity (with corresponding changes in ϕ_*).

on angular scales out to several arcminutes, much larger than potential host galaxies. The *IRAS* photometry is susceptible to missing extended emission, but for PSCz galaxies this has been corrected for (Saunders et al. 2000), and in any case any missing *IRAS* flux would lower the FIR to radio ratio, which is in the opposite sense to the observed differences. More likely is that there is a genuine effect at work: either the radio luminosity or the FIR luminosity is not directly proportional to the star formation. One way in which this might occur is if there is an additional low-level contribution to the FIR luminosity of galaxies, for example from dust heated by low mass stars, which is usually swamped by the FIR emission associated with star formation, but becomes significant at low star formation rates (cf. Devereux & Eales 1989 and references therein).

6 CONCLUSIONS

The main results of this paper are as follows.

(i) A catalogue of 2712 radio sources has been derived by cross-correlating the SDSS spectroscopic sample with a combination of the NVSS and FIRST surveys.

(ii) The use of a hybrid NVSS–FIRST method to identify the radio sources has been highly successful, resulting in a sample with a reliability of 98.9 per cent and a completeness which is estimated to be over 95 per cent.

(iii) The radio sources have been sub-divided into 2215 radio-loud AGN and 497 star-forming galaxies, based upon their location in the plane of 4000-Å break strength versus radio luminosity per unit stellar mass.

(iv) The local radio luminosity functions of radio-loud AGN and star-forming galaxies have been derived separately. These are in excellent agreement with previous studies, but with smaller uncertainties.

(v) The local radio luminosity function of star-forming galaxies has been compared to that derived in the FIR. Differences between the two confirm that the FIR to radio correlation becomes non-linear at low luminosities.

The development of the hybrid NVSS–FIRST method for identification of radio sources represents a large step forward in the study of radio source host galaxies. One note of caution needs to be added: the parameters for acceptance or rejection of sources have been optimized for the SDSS spectroscopic sample, and if the comparison survey has a significantly different sky surface density of objects, the offset parameters for acceptance may need to be modified in order to retain optimal completeness and reliability. The general method, however, can (and where possible, should) be adopted unchanged in future studies.

The sample of radio sources produced will prove invaluable in the study of the host galaxies of radio-loud AGN, due to the large size of the sample and the wealth of information available on the host galaxies from the SDSS. Such analysis is the focus of the accompanying paper.

REFERENCES

Baldwin J. A., Phillips M. M., Terlevich R., 1981, PASP, 93, 5 (BPT)
Becker R. H., White R. L., Helfand D. J., 1995, ApJ, 450, 559
Best P. N., 2004, MNRAS, 351, 70
Best P. N., Kauffmann G., Heckman T. M., Brinchmann J., Charlot S., Ivezić Ž., White S. D. M., 2005, MNRAS, in press (doi:10.1111/j.1365-2966.2005.09192) (this issue)
Brinchmann J., Charlot S., Heckman T., Kauffmann G., Tremonti C., White S. D. M., 2004a, http://www.mpa-garching.mpg.de/SDSS (astro-ph/0406220)
Brinchmann J., Charlot S., White S. D. M., Tremonti C., Kauffmann G., Heckman T., Brinkmann J., 2004b, MNRAS, 351, 1151
Bruzual G., Charlot S., 2003, MNRAS, 344, 1000
Carilli C. L., 2001, in Tacconi L., Lutz D., eds, Starburst Galaxies: Near and Far. Springer-Verlag, Berlin, p. 309
Colless M. M. et al., 2001, MNRAS, 328, 1039
Condon J. J., 1989, ApJ, 338, 13
Condon J. J., 1992, ARA&A, 30, 575
Condon J. J., Cotton W. D., Greisen E. W., Yin Q. F., Perley R. A., Taylor G. B., Broderick J. J., 1998, AJ, 115, 1693
Devereux N. A., Eales S. A., 1989, ApJ, 340, 708
Heckman T. M., Kauffmann G., Brinchmann J., Charlot S., Tremonti C., White S. D., 2004, ApJ, 613, 109
Hopkins A. M., Connolly A. J., Haarsma D. B., Cram L. E., 2001, AJ, 122, 288
Ivezić Ž. et al., 2002, AJ, 124, 2364
Kauffmann G. et al., 2003a, MNRAS, 341, 33
Kauffmann G. et al., 2003b, MNRAS, 341, 54
Kauffmann G. et al., 2003c, MNRAS, 346, 1055
Machalski J., Condon J. J., 1999, ApJ, Supp., 123, 41
Machalski J., Godlowski W., 2000, A&A, 360, 463

Magliocchetti M., Maddox S. J., Lahav O., Wall J. V., 1998, MNRAS, 300, 257
McMahon R. G., White R. L., Helfand D. L., Becker R. H., 2002, ApJ, Supp., 143, 1
Sadler E. M. et al., 2002, MNRAS, 329, 227
Sandage A., Tammann G. A., Yahil A., 1979, ApJ, 232, 352
Saunders W. et al., 2000, MNRAS, 317, 55
Schmidt M., 1968, ApJ, 151, 393
Shectman S. A., Landy S. D., Oemler A., Tucker D. L., Lin H., Kirshner R. P., Schechter P. L., 1997, ApJ, 470, 172
Stoughton C. et al., 2002, AJ, 123, 485
Takeuchi T. T., Yoshikawa K., Ishii T. T., 2003, ApJ, 587, L89

Tremonti C. A. et al., 2004, ApJ, 613, 898
York D. G. et al., 2000, AJ, 120, 1579
Yun M. S., Reddy N. A., Condon J. J., 2001, ApJ, 554, 803

7 SUPPLEMENTARY MATERIAL

The following supplementary material is available for this article online:
Table 2. Properties of the 2712 SDSS radio galaxies.

This paper has been typeset from a TEX/LATEX file prepared by the author.